Cell Research

www.nature.com/cr
www.cell-research.com

ARTICLE

Binding pathway determines norepinephrine selectivity for the human β_1AR over β_2AR

Xinyu Xu[1,2], Jonas Kaindl[3], Mary J. Clark[4], Harald Hübner[3], Kunio Hirata[5,6], Roger K. Sunahara[4], Peter Gmeiner[3], Brian K. Kobilka[1,2,7] and Xiangyu Liu[1,8]

Beta adrenergic receptors (βARs) mediate physiologic responses to the catecholamines epinephrine and norepinephrine released by the sympathetic nervous system. While the hormone epinephrine binds β_1AR and β_2AR with similar affinity, the smaller neurotransmitter norepinephrine is approximately tenfold selective for the β_1AR. To understand the structural basis for this physiologically important selectivity, we solved the crystal structures of the human β_1AR bound to an antagonist carazolol and different agonists including norepinephrine, epinephrine and BI-167107. Structural comparison revealed that the catecholamine-binding pockets are identical between β_1AR and β_2AR, but the extracellular vestibules have different shapes and electrostatic properties. Metadynamics simulations and mutagenesis studies revealed that these differences influence the path norepinephrine takes to the orthosteric pocket and contribute to the different association rates and thus different affinities.

Cell Research (2021) 31:569–579; https://doi.org/10.1038/s41422-020-00424-2

INTRODUCTION

The beta-adrenergic receptors (βARs) belong to the G protein-coupled receptor (GPCR) family. As part of the sympathetic nervous system, βARs mediate physiological responses to the catecholamines norepinephrine and epinephrine to regulate cardiovascular, respiratory and metabolic functions. Norepinephrine is a neurotransmitter released from sympathetic nerves, whereas epinephrine is a hormone primarily released from the adrenal medulla into the systemic circulation. β_1AR and β_2AR are highly homologous and both are expressed in the heart,[1] but they play distinct roles in regulating cardiac function. While these receptors have the same affinity for epinephrine, the β_1AR has a tenfold higher affinity for norepinephrine than the β_2AR. While both β_1AR and β_2AR activate Gs leading to activation of adenylyl cyclase and an increase in cAMP, they reside in distinct signaling domains in cardiac myocytes,[2–5] which may contribute to their distinct roles in cardiac physiology.[6–8] Epinephrine-activated β_2AR also couples to Gi in cardiac myocytes, which inhibits adenylyl cyclase. In addition to having a lower affinity for the β_2AR, norepinephrine does not promote coupling to Gi in cardiac myocytes.[9] As discussed below, the differences in norepinephrine affinity and G protein coupling specificity suggest that the β_2AR plays a minor role in physiologic regulation of cardiac function, but is protective in pathologic stress.

The sympathetic nervous system regulates cardiovascular response to changes in body position (supine to erect) and activity (sitting to walking and running). Under normal physiologic conditions, cardiovascular function is regulated primarily by norepinephrine released from sympathetic nerve terminals. Consistent with this, the major circulating catecholamine is norepinephrine that is released from sympathetic nerves and escapes into the circulation before undergoing reuptake at the synapse.[10] Under more severe stress such as fight or flight, hypotension from hemorrhage or sepsis, or loss of cardiac function from infarction or heart failure, the adrenal gland releases epinephrine into circulation where it becomes the major circulating hormone.[10] Thus, under normal physiologic conditions cardiac β_2ARs contribute relatively little toward cardiac function because of their lower affinity for norepinephrine, their location relative to the sympathetic synapse,[2] and the fact that norepinephrine promotes coupling of β_2AR only to Gs, and not Gi. Under these physiologic conditions, coupling to Gi would be expected to antagonize the effects of Gs activation in enhancing cardiac performance. However, under extreme and prolonged stress, stimulation of the β_1AR by high levels of epinephrine and norepinephrine leads to cardiac myocyte apoptosis, necrosis and remodeling,[11,12] while stimulation of the β_2AR leads to activation of anti-apoptosis and anti-necrosis pathways to protect the heart.[13–16] The cardioprotective effects of β_2AR activation can be inhibited by disrupting β_2AR-Gi signaling, converting β_2AR activation from anti-apoptotic to pro-apoptotic.[14]

Thus, β_2AR activation is beneficial under conditions of prolonged pathologic stress to protect the heart, but should be minimized under physiological conditions to avoid opposing

[1]Beijing Advanced Innovation Center for Structural Biology, Tsinghua University, Beijing 100084, China; [2]School of Medicine, Tsinghua University, Beijing 100084, China; [3]Department of Chemistry and Pharmacy, Medicinal Chemistry, Friedrich–Alexander University Erlangen–Nürnberg, Nikolaus-Fiebiger-Straße 10, Erlangen 91058, Germany; [4]Department of Pharmacology, University of California San Diego School of Medicine, 9500 Gilman Drive, La Jolla, CA 92093, USA; [5]Advanced Photon Technology Division, Research Infrastructure Group, SR Life Science Instrumentation Unit, RIKEN/SPring-8 Center, 1-1-1 Kouto Sayo-cho Sayo-gun, Hyogo 679-5148, Japan; [6]Precursory Research for Embryonic Science and Technology (PRESTO), Japan Science and Technology Agency, 4-1-8 Honcho, Kawaguchi, Saitama 332-0012, Japan; [7]Department of Molecular and Cellular Physiology, Stanford University School of Medicine, Stanford, CA 94305, USA and [8]School of Pharmaceutical Sciences, Tsinghua University, Beijing 100084, China
Correspondence: Roger K. Sunahara (rsunahara@ucsd.edu) or Peter Gmeiner (peter.gmeiner@fau.de) or Xiangyu Liu (liu_xy@mail.tsinghua.edu.cn)
These authors contributed equally: Xinyu Xu, Jonas Kaindl, Mary J. Clark

Received: 5 June 2020 Accepted: 28 September 2020
Published online: 22 October 2020

β_1AR-mediated cardiac regulation through β_2AR coupling to Gi or contribute to cardiotoxicity through β_2AR coupling to Gs. Therefore, the lower affinity of the β_2AR for norepinephrine appears to play an important role in cardiac physiology. This difference is surprising given that norepinephrine is only slightly smaller than epinephrine, which has the same affinity for both subtypes, and the amino acids that form the orthosteric binding pocket for epinephrine (defined here as within 4 Å of epinephrine bound to the β_2AR) are identical for the β_1AR and β_2AR.

The human β_2AR[17–19] and turkey β_1AR[20,21] were among the first hormone-activated GPCR structures to be determined. So far, there are over 50 structure entries of the human β_2AR and turkey β_1AR bound to different agonists and antagonists in the protein data bank, yet none of these structures captured a complex between the receptor and norepinephrine. Despite the high sequence homology between the human β_1AR, the turkey β_1AR, and the human β_2AR, these βARs have different pharmacologic properties (Supplementary information, Fig. S1).[22] Structural information can explain the selectivity mechanism for ligands like the β_2AR-selective salmeterol, that extend out of the orthosteric binding pocket into the more divergent extracellular vestibule.[23] However, existing structures cannot explain the tenfold selectivity of norepinephrine for the human β_1AR over the human β_2AR, where the binding pockets are expected to be identical. Understanding the mechanism of the β_1AR selectivity of norepinephrine may aid in the development of subtype-selective drugs not only for βARs, which are the primary drug targets of cardiovascular and pulmonary diseases, but also for other GPCRs. Factors that contribute to the affinity, but not evident in the crystal structure, include the rates of ligand association and dissociation.[24] We therefore sought to investigate the molecular mechanism of norepinephrine selectivity for the human β_1AR using binding kinetics studies, structural biology and metadynamics simulations.

RESULTS

Association rate determines selectivity of norepinephrine

The binding affinity is determined by both association rate (K_{on}) and dissociation rate (K_{off}). We measured the binding kinetics of norepinephrine to both human β_1AR and β_2AR using competition association binding assays. Norepinephrine displayed faster association rates (on-rates, ~22-fold) but comparable dissociation rates (off-rate, ~1.5-fold) for the β_1AR over the β_2AR. The combined effects on the association and dissociation rate result in a lower K_d for norepinephrine for the β_1AR, and agree with K_i measured in competition assays at equilibrium. While binding affinity differences can usually be attributed to differences in the dissociation rate, our results suggest that differences in the affinity of β_1AR and β_2AR for norepinephrine are mainly determined by the differences in on-rates (Fig. 1a; Supplementary information, Table S1).

Given that the residues forming the catecholamine-binding pockets are identical between the β_1AR and β_2AR, we explored the role of the differences in the amino acid composition and thus shape of the extracellular vestibules. Two chimeric constructs were generated; one with the transmembrane core of the β_1AR and extracellular vestibule of the β_2AR (hereby named $\beta_1AR_{in}/\beta_2AR_{out}$), the other contains the transmembrane core of the β_2AR and extracellular vestibule of the β_1AR (hereby named $\beta_2AR_{in}/\beta_1AR_{out}$) (Fig. 1b; Supplementary information, Fig. S2). Binding kinetics studies on these two chimeric receptors were performed (Fig. 1a). Accordingly, the $\beta_2AR_{in}/\beta_1AR_{out}$ chimera showed a much faster

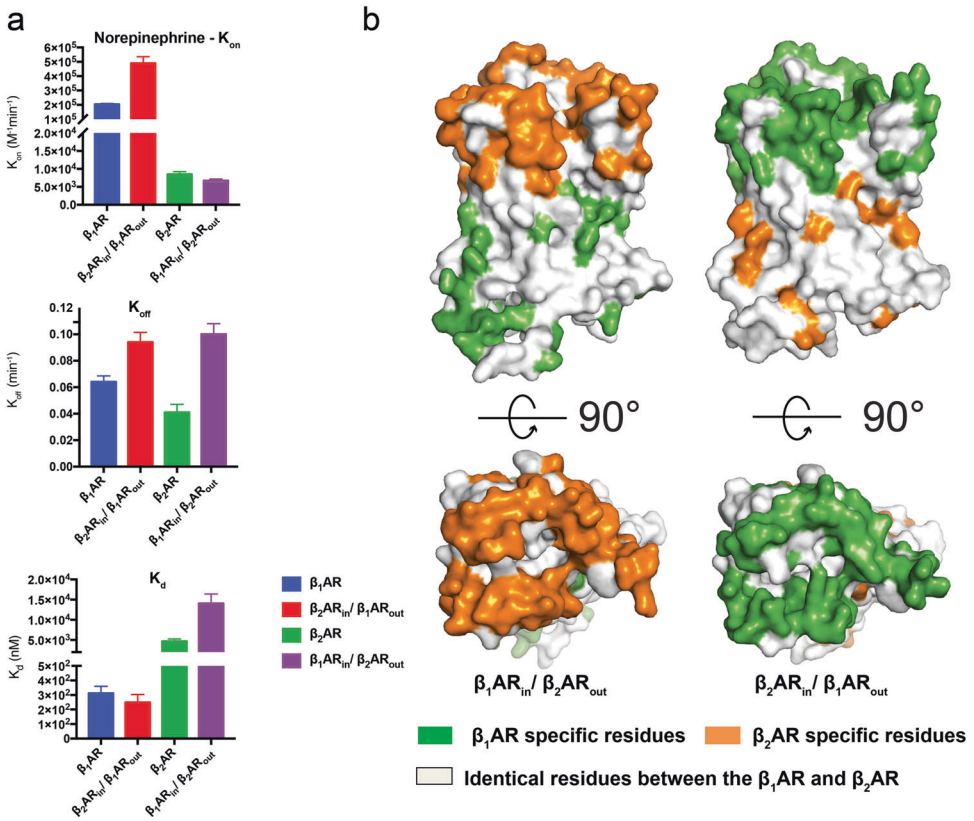

Fig. 1 Kinetics studies of norepinephrine binding to the β_1AR, β_2AR and $\beta_1AR_{in}/\beta_2AR_{out}$, $\beta_2AR_{in}/\beta_1AR_{out}$ chimeras. a Comparison of the K_{on}, K_{off} and K_d of norepinephrine to the β_1AR, β_2AR and $\beta_1AR_{in}/\beta_2AR_{out}$, $\beta_2AR_{in}/\beta_1AR_{out}$ chimeras. Data are given as means ± SEM of 3–8 independent experiments. **b** Design of the $\beta_1AR_{in}/\beta_2AR_{out}$, $\beta_2AR_{in}/\beta_1AR_{out}$ chimeras.

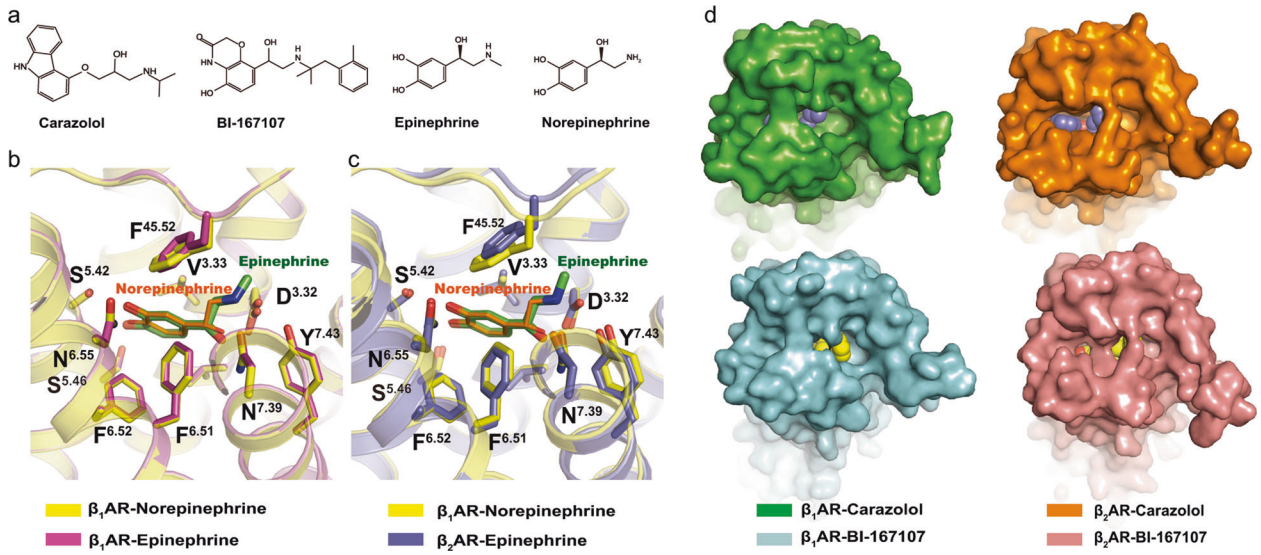

Fig. 2 Comparison of the orthosteric pockets and extracellular vestibules between the human β_1AR and β_2AR. a Chemical structures of the following β_1AR ligands: inverse agonist carazolol, high-affinity agonist BI-167107, endogenous catecholamines epinephrine and norepinephrine. **b** Comparison of the orthosteric pockets of β_1AR–norepinephrine structure (yellow) and β_1AR–epinephrine (magenta) structure. **c** Comparison of the orthosteric pockets of β_1AR–norepinephrine structure (yellow) and β_2AR–epinephrine (blue, PDB code: 4LDO) structure. **d** Comparison of the extracellular vestibules of inactive (carazolol-bound, green) and active (BI-167107-bound, cyan) β_1AR with inactive (carazolol-bound, PDB code: 2RH1, orange) and active (BI-167107-bound, PDB code: 4LDE, pink) β_2AR structures.

on-rate than β_2AR (~60-fold) and $\beta_1AR_{in}/\beta_2AR_{out}$ chimera showed a slower on-rate than β_1AR (~30-fold). This suggest that the extracellular vestibules of the β_1AR and β_2AR are the key determinants of the different association rates of norepinephrine to the receptors, and thus of the different affinities. Interestingly, the chimeric receptor $\beta_2AR_{in}/\beta_1AR_{out}$ displays an even faster association rate and higher affinity for norepinephrine than the wild-type β_1AR. This may in part be due to the higher basal activity of β_2AR compared to β_1AR.[25] The transmembrane core of β_2AR might affect the equilibrium between inactive (low agonist affinity) and active (high agonist affinity) states; thereby allosterically affect the shape of the β_1AR extracellular vestibule. In the β-arrestin recruitment assay, the EC50 values of the ligands to the different receptor constructs are in agreement with the ligand affinities measured in the study (Supplementary information, Fig. S3), the results suggest that mutating the extracellular surface does not interfere with the signal transduction at the intracellular side, since the residues involved in the downstream singling remain unchanged.

Shape of the extracellular vestibule differs between β1AR and β2AR

Delineating structural information on the extracellular vestibules is the key to understand the molecular mechanism of the different norepinephrine association rates between the human β_1AR and β_2AR. High-resolution structures of the human β_2AR in inactive and active states have been solved,[18,26,27] including β_2AR bound to epinephrine.[28] We therefore determined the structures of the human β_1AR in both inactive and active conformations, bound to an antagonist (carazolol) and agonists (BI-167107, epinephrine and norepinephrine), respectively (Fig. 2a; Supplementary information, Fig. S4a, b). The crystal structure resolutions range from 2.5 to 3.1 Å (Supplementary information, Table S2). Clear densities of the ligands are revealed by fo-fc simulated annealing omit maps (Supplementary information, Fig. S5).

The inactive and active β_1AR structures display remarkable overall similarity to those of the β_2AR. The classical structural change associated with receptor activation, the outward movement of TM5 and TM6 and the inward displacement of TM3 and TM7 on the cytoplasmic side, are also observed in β_1AR structures. The features for conformational change also include the rearrangement of $P236^{5.50}$, $I246^{3.40}$ and $F333^{6.44}$, representing the conserved PIF motif (Supplementary information, Fig. S4c, d), as well as the water-mediated hydrogen bond between $Y^{5.58}$ and $Y^{7.53}$ in the NPxxY motif (Supplementary information, Fig. S4e, f).

As expected, the catecholamine-binding pockets are similar between the β_1AR and β_2AR. When comparing the β_1AR-norepinephrine and β_1AR–epinephrine structures, the orthosteric binding pockets are almost identical. The additional methyl group of epinephrine is accommodated without any notable side chain rearrangement (Fig. 2b). When comparing the β_1AR-norepinephrine structure with the β_2AR–epinephrine structure (PDB: 4LDO), all of the orthosteric binding pocket residues occupy similar positions, except for slightly different conformation of $F^{45.52}$ in the ECL2 (Fig. 2c). However, we are not certain if the conformational difference of $F^{45.52}$ observed in the crystal structure is due to real conformational differences or due to local energy minimum of receptors affected by different crystallization conditions. Unbiased Molecular dynamics (MD) simulations (3×4 μs, each) did not reveal significant differences of $F^{45.52}$ rotamers (Supplementary information, Fig. S6). This observation is consistent with the fact that the affinity of epinephrine is the same for β_1AR and β_2AR.

MD simulations of norepinephrine bound to the β_2AR reveal a similar pose as observed in the β_1AR crystal structure (Supplementary information, Fig. S4g, h). Hence, the binding poses do not explain the higher affinity of norepinephrine towards β_1AR. Comparison of the extracellular vestibules of β_1AR and β_2AR reveals considerable structural differences, suggesting that differences in the connection between solvent and the orthosteric pocket may account for their differing affinities for norepinephrine (Fig. 2d).

Norepinephrine takes different paths to bind to β1AR and β2AR

To investigate how the different structures of the extracellular vestibule affect norepinephrine binding, we sought to understand the mechanism of ligand recognition by β_1AR and β_2AR using simulations. As ligand binding events tend to occur on time scales typically not broadly accessible by unbiased MD simulations, metadynamics simulations were performed to calculate the ligand

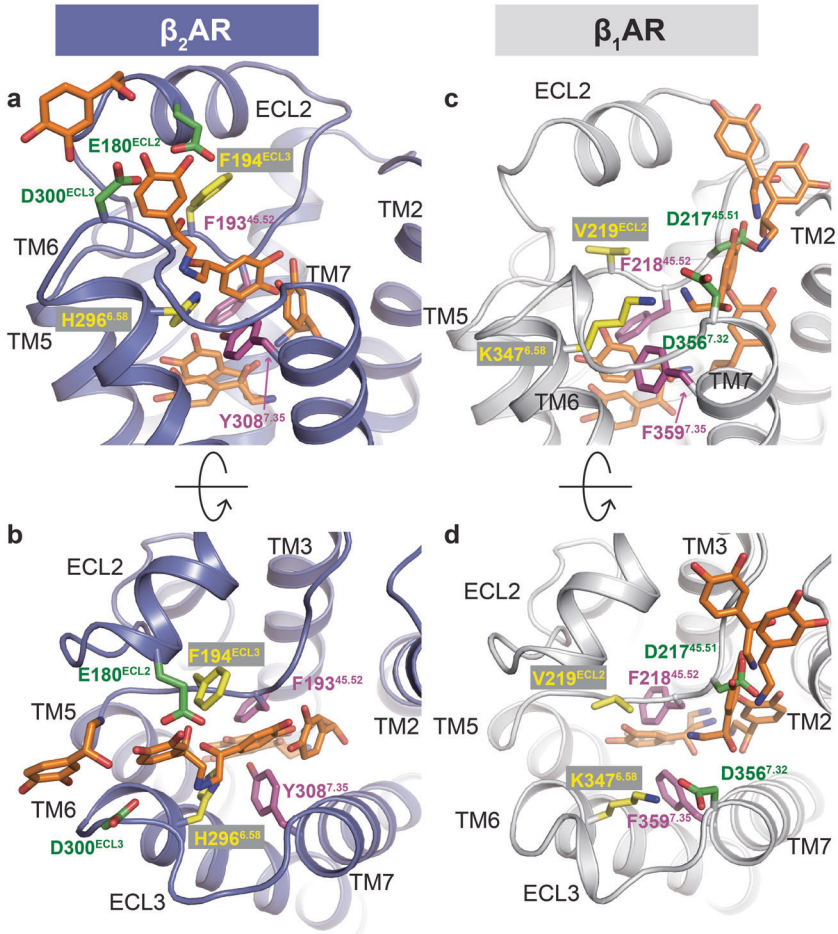

Fig. 3 Metadynamics simulations reveal different norepinephrine entrance pathway in the β_1AR and β_2AR. a Side view of the norepinephrine-binding pathway in the β_2AR. Norepinephrine first interacts with the receptor through two negatively charged residues (green), then moves through a tunnel formed by F194^{ECL2} and H296$^{6.58}$ (yellow), then enters the orthosteric pocket by passing through a gate formed by two aromatic residues (purple). **b** Top view of the norepinephrine-binding pathway in the β_2AR. **c** Side view of the norepinephrine-binding pathway in the β_1AR. Norepinephrine first interacts with the receptor through two negatively charged residues (green). Before entering the orthosteric pocket, norepinephrine needs to pass through a gate formed by two aromatic residues (purple). **d** Top view of the norepinephrine-binding pathway in the β_1AR.

entrance pathway using an established protocol to investigate the interaction of small molecules and GPCRs.[29] Here, the protonated and thus positively charged states of norepinephrine and epinephrine and the inactive-state conformation of the two receptors were applied, as the extracellular sites of inactive-state receptors are expected to better resemble the unoccupied, non-G protein-coupled form of the receptors.[30]

Interestingly, the simulations suggest that norepinephrine takes different pathways to the orthosteric binding pockets in the β_1AR and β_2AR (Fig. 3). For the β_2AR, norepinephrine first contacts the receptor through two negatively charged residues E180^{ECL2} and D300^{ECL3} located on the TM6 side of the ECL2/ECL3 vestibule (Fig. 3a, b, green residues), then moves through a tunnel formed by F194^{ECL2} and H296$^{6.58}$ (Fig. 3a, b, yellow residues) to the TM2 side of the ECL2/ECL3 vestibule. To enter the final orthosteric pocket, norepinephrine needs to pass through a gate formed by the two aromatic residues F193$^{45.52}$ and Y308$^{7.35}$ (Fig. 3a, b, purple residues). The results agree well with the previously simulated alprenolol-binding pathway.[31] As with the β_2AR, norepinephrine also initially interacts with the β_1AR through two negatively charged residues, D217$^{45.51}$ and D356$^{7.32}$ (Fig. 3c, d, green residues) and also needs to pass through two aromatic residues F218$^{45.52}$ and F359$^{7.35}$ (Fig. 3c, d, purple residues) to enter the orthosteric pocket. However, D217$^{45.51}$ and D356$^{7.32}$ are close to the TM2 side of the ECL2/ECL3 vestibule and as a result, norepinephrine does not need to move from one side of the ECL2/ECL3 vestibule to the other side in the β_1AR.

Subtype-specific differences in the binding pathways

To ascertain why norepinephrine appears to take different pathways in these two receptors, the residues that may affect the ligand-binding process were thus interrogated. The well-studied turkey β_1AR, which has a sequence identity of 82% to the human β_1AR for the residues W57$^{1.31}$–D259$^{5.73}$ and E319$^{6.30}$–C392$^{8.59}$ (the entire receptor excluding the N- and C-termini, as well as a part of ICL3), was also added to the analysis.

A pair of negatively charged residues and a salt bridge between the ECL2 and ECL3 are found in all the three receptors (Fig. 4a–c). The negatively charged residue pair where norepinephrine first interacts with the receptor is conserved in the human β_1AR (D217$^{45.51}$ and D356$^{7.32}$) and turkey β_1AR (D200$^{45.51}$ and D322$^{7.32}$), and is in a different position in the human β_2AR (E180^{ECL2} and D300^{ECL3}). The salt bridges are in different positions in the three receptors; they are formed by E205^{ECL2} and R351^{ECL3} in the human β_1AR, by D192$^{45.51}$ and K305$^{7.32}$ in the human β_2AR, and by D184^{ECL2} and R317^{ECL3} in the turkey β_1AR.

The F194^{ECL2} and H296$^{6.58}$ pair that coordinates norepinephrine entrance in the human β_2AR is not conserved in either human

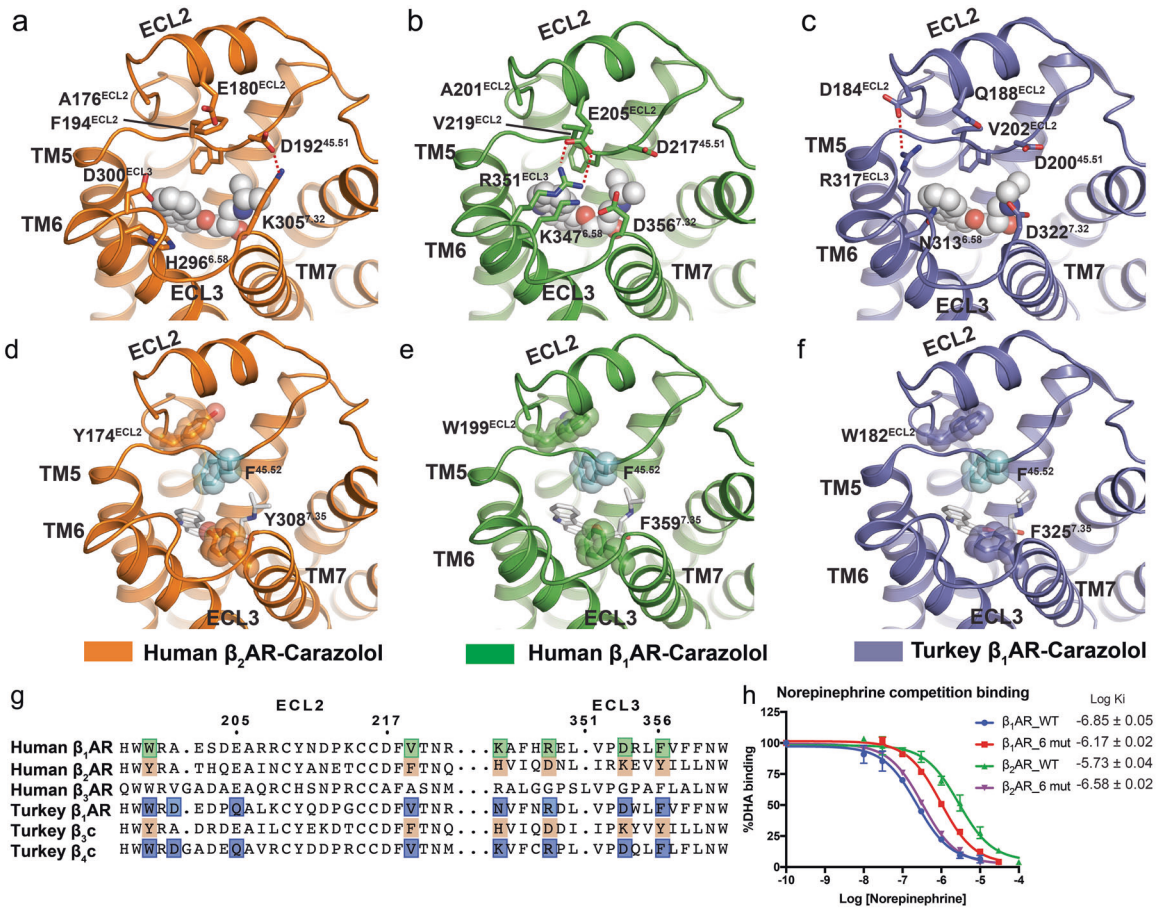

Fig. 4 Analysis of different residues on the extracellular domain of the receptors that contribute to the different norepinephrine-binding pathway. a The negatively charged residue pair (E180^{ECL2} and D300^{ECL3}) and salt bridge (D192$^{45.51}$ and K305$^{7.32}$) between the ECL2 and ECL3 of the human β_2AR (PDB code: 2RH1). **b** The negatively charged residue pair (D217$^{45.51}$ and D356$^{7.32}$) and salt bridge (E205^{ECL2} and R351^{ECL3}) between the ECL2 and ECL3 of the human β_1AR. **c** The negatively charged residue pair (D200$^{45.51}$ and D322^{ECL3}) and salt bridge (D184^{ECL2} and R317^{ECL3}) between the ECL2 and ECL3 of the turkey β_1AR (PDB code: 2YCW). **d** The conserved F$^{45.52}$ (cyan) is surrounded by two aromatic residues Y174^{ECL2} and Y308$^{7.35}$ in the human β_2AR (PDB code: 2RH1). **e** The conserved F$^{45.52}$ (cyan) is surrounded by two aromatic residues W199^{ECL2} and F359$^{7.35}$ in the human β_1AR. **f** The conserved F$^{45.52}$ (cyan) is surrounded by two aromatic residues W182^{ECL2} and F325$^{7.35}$ in the turkey β_1AR (PDB code: 2YCW). **g** Sequence alignment of ECL2 and ECL3 of the three human βARs and three turkey βARs. The residues that account for the different ligand entrance pathway are highlighted. **h** Mutating the six residues aligning the ligand entrance pathway of the β_1AR to their counterparts in the β_2AR (β_1AR_6mut) decreased norepinephrine affinity, while the reverse mutations of the β_2AR (β_2AR_6mut) increased norepinephrine affinity. Data are given as means ± SEM from three independent experiments performed in duplicate. The concentrations of [^{3}H]-DHA for competition binding are varied from 0.15 to 0.9 nM based on the K_d for the distinct constructs.

β_1AR (V219^{ECL2} and K347$^{6.58}$) or turkey β_1AR (V202^{ECL2} and N313$^{6.58}$). The final aromatic gate through which norepinephrine enters the orthosteric pocket in the human β_2AR is formed by a Phe (F193$^{45.52}$) and a Tyr (Y308$^{7.35}$). In both the human and turkey β_1AR, the gate is formed by two Phe residues (F218$^{45.52}$ and F359$^{7.35}$ and F201$^{45.52}$ and F325$^{7.35}$, respectively). Interestingly, there is another aromatic residue on ECL2 that is within 4 Å distance of F$^{45.52}$ and may affect the conformation or dynamics of F$^{45.52}$, which is a Tyr in the human β_2AR (Y174^{ECL2}) and a Trp in the human and turkey β_1AR (W199^{ECL2} and W182^{ECL2}, respectively) (Fig. 4d–f).

Sequence alignment suggests eight residues on the extracellular side of the human β_1AR, the human β_2AR and the turkey β_1AR contribute toward the different shapes of the extracellular vestibule of the receptors (Fig. 4g). Comparing the sequences of all three human βARs and the three turkey βARs at these eight positions reveals that the turkey β_{3C}AR is identical to the human β_2AR in all eight positions, while the turkey β_{4C}AR has seven residues in common with the turkey β_1AR and has a similar salt bridge between ECL2 and ECL3 as the turkey β_1AR. The human β_1AR and β_3AR are more different compared to the other four subtypes (Fig. 4g). Interestingly, a full pharmacology study of these six receptors suggests that turkey β_{3C}AR has a pharmacological profile similar to the human β_2AR, and the turkey β_{4C}AR is more similar to the turkey β_1AR. Of note, these six βARs have identical orthosteric pocket residues[22] (Supplementary information, Fig. S7).

Functional characterization of binding pathway mutations

Out of the above-mentioned eight residues, six residues are different between the human β_1AR and β_2AR, which are W199^{ECL2}, V219^{ECL2}, K347$^{6.58}$, R351^{ECL3}, D356$^{7.32}$ and F359$^{7.35}$ in the human β_1AR and Y174^{ECL2}, F194^{ECL2}, H296$^{6.58}$, D300^{ECL3}, K305$^{7.32}$ and Y308$^{7.35}$ in the human β_2AR. To determine whether the six amino acids define the entry path to the orthosteric site, and are responsible for norepinephrine's selectivity for β_1AR over β_2AR, we characterized the pharmacology of mutants where the six residues were exchanged between the receptor subtypes. Substituting all six residues in β_2AR with those of β_1AR (β_2AR-6mut) led to an enhanced affinity for norepinephrine (Fig. 4h). Further mutagenesis studies indicate that all six substitutions were minimally required to observe norepinephrine's enhanced affinity

(Supplementary information, Fig. S8). In contrast, while substituting all six residues in β_1AR with those of β_2AR (β_1AR-6mut) decreases norepinephrine affinity (Fig. 4h), different combinations of three mutations produce a near-maximal decrease in affinity (Supplementary information, Fig. S8). The β_1AR-F359Y showed the largest decrease on norepinephrine affinity among the 6 single mutations of the β_1AR (Supplementary information, Fig. S8a), but the reverse mutation in the β_2AR (β_2AR-Y308F) did not show any increase in norepinephrine affinity (Supplementary information, Fig. S8c) and a combination of mutations were required to increase norepinephrine affinity in the β_2AR, including a mutant without the Y308F mutation (β_2AR-5mut-1) (Supplementary information, Fig. S8d). Similar results were reported for mutagenesis studies in turkey β_1AR and human β_2AR.[21] Furthermore, a triple mutant (β_1AR-3mut-3) without the F359Y mutation showed a comparable effect in decreasing norepinephrine affinity as the β_1AR-6mut (Supplementary information, Fig. S8b). The complex behaviors of the mutants suggest that norepinephrine selectivity is determined by a combination of residues that cooperate to form the ligand-binding pathway (Supplementary information, Fig. S8). It should be noted that the β_1AR-6mut and β_1AR have similar affinities for epinephrine, while the β_2AR-6mut has a slightly (less than threefold) increased affinity for epinephrine compared to the β_2AR (Supplementary information, Fig. S9). Similar results are obtained with the β-arrestin recruitment assay where both epinephrine and norepinephrine maintain full agonist activity for the β_1AR, β_2AR, β_1AR_6mut and β_2AR_6mut receptors, but with different EC50 values in agreement with the K_i values measured in the binding assay (Supplementary information, Fig. S10). The results suggest the six residue mutations do not affect the overall conformation of the orthosteric binding pocket or the downstream signaling. Binding kinetics studies confirmed that mutating the six residues mainly affect the association rate of norepinephrine, the K_{on} of norepinephrine is ~7-fold lower in β_1AR-6mut compared to β_1AR, and ~16-fold higher in β_2AR-6mut compared to β_2AR (Supplementary information, Table S1). Of note, the fold-change in the association rate (and affinity) of norepinephrine for β_1AR-6mut, or the β_2AR-6mut, is not as large nor as

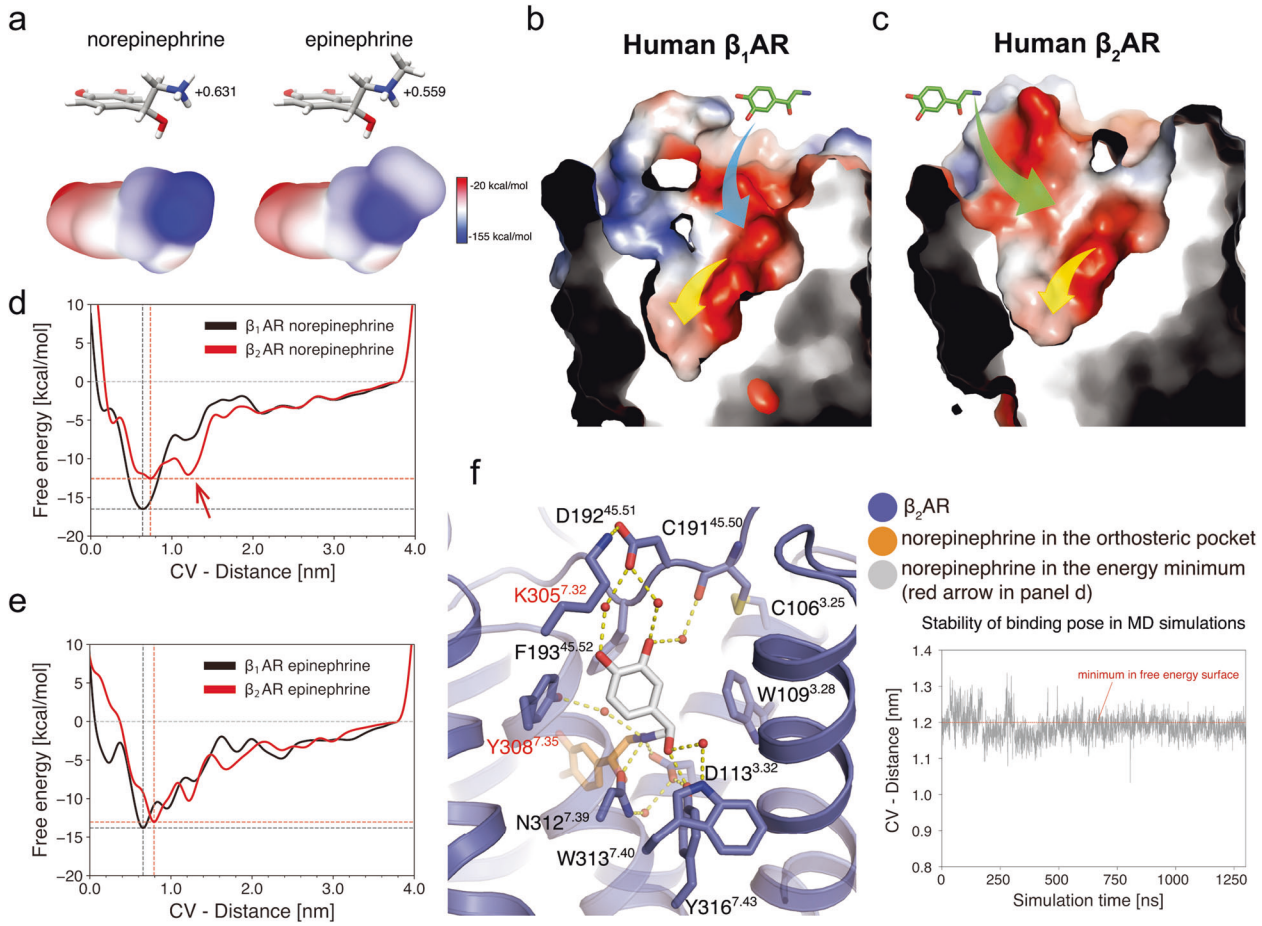

Fig. 5 Epinephrine does not have preference for the β_1AR or the β_2AR as norepinephrine does due to difference in electrostatic properties. a Comparison of partial charge of the protonated nitrogen and charge distribution of norepinephrine and epinephrine. Illustrated are the electrostatic potential charges of the two nitrogens, based on the sum of partial charges of the nitrogen and its attached hydrogen. The MEP is mapped onto the quantum mechanical isodensity surface (0.001 au) of norepinephrine and epinephrine, respectively. **b** The ligand-binding pathway of the human β_1AR is composed of a continuous negatively charged tunnel. **c** The ligand-binding pathway of the human β_2AR is composed of two negatively charged areas connected by a neutral gap. **d** The norepinephrine-binding energy profiles are different between the β_1AR and β_2AR. The red arrow indicates a local energy minimum of norepinephrine–β_2AR complex at a CV distance of 1.2 nm. **e** The epinephrine-binding energy profiles show similar patterns in the β_1AR and β_2AR. **f** Snapshot of metadynamics simulations illustrating norepinephrine–β_2AR complex for energy minimum at CV distance of 1.2 nm. Norepinephrine is engaged in an extensive hydrogen network with D113$^{3.32}$, N312$^{7.39}$ and Y316$^{7.43}$, and water-mediated interactions to C191$^{45.50}$, D192$^{45.51}$, K305$^{7.32}$, Y308$^{7.35}$, and W313$^{7.40}$. Of these residues, K305$^{7.32}$ and Y308$^{7.35}$ are different between the β_1AR and β_2AR (labeled in red font). The plot shows the distance representing the collective variable applied during metadynamics simulations during unbiased MD of norepinephrine in complex with β_2AR. Norepinephrine maintains the binding mode for 1275 ns in unbiased MD simulations.

complete as with the $\beta_1AR_{in}/\beta_2AR_{out}$ or $\beta_2AR_{in}/\beta_1AR_{out}$ chimeric receptors, which were constructed by exchanging the N-terminus (from the first residue to $W^{1.31}$) plus another 55 amino acids on the extracellular half of the receptor that differ between the β_1AR and β_2AR (Fig. 1b; Supplementary information, Fig. S2). We speculate that other regions of the extracellular face contained in the chimeric receptors, but more distant from the orthosteric pocket may influence the electrostatic potential of the receptor, alter the conformation equilibrium between active and inactive states, or influence the overall shape of the extracellular vestibule (Supplementary information, Fig. S11).

The results suggest the existence of allosteric effects where other regions of the receptor may affect the conformation or dynamics of the residues forming the ligand-binding pathway or orthosteric pocket and thus affect the ligand affinity. To examine such an allosteric effect, we chose $F^{45.52}$ as an example to perform mutagenesis studies. $F^{45.52}$ is an important part of the entrance pathway and orthosteric pocket for both β_1AR and β_2AR. The residue is conserved as Phe in both the β_1AR and β_2AR, but several of the residues surrounding $F^{45.52}$ are different between the two receptors (Fig. 4a–f) and as a result, $F^{45.52}$ may have different conformational and dynamics properties, and play different roles in ligand affinities in the β_1AR and β_2AR. Indeed, while the $F^{45.52}A$ mutation only slightly reduced norepinephrine affinity for the β_2AR (approximately threefold decrease in K_i value), it reduced affinity for the β_1AR by more than 250-fold (Supplementary information, Fig. S12). Molecular dynamics studies suggest that the $F^{45.52}A$ mutation has a greater impact on the binding pathway for the β_1AR than for the β_2AR (Supplementary information, Fig. S13). The $F^{45.52}A$ mutation results in a higher fluctuation of ECL2 in the β_1AR and higher fluctuation of ECL3 in the β_2AR (Supplementary information, Fig. S13). Interestingly, $F^{45.52}A$ mutation induces alternative conformations of $D217^{45.51}$ only in the β_1AR, but not in the β_2AR. As mentioned earlier, $D217^{45.51}$ is part of the negatively charged residue pair where norepinephrine first interacts with the receptor. The results may explain why $F^{45.52}A$ mutation has larger effects on norepinephrine affinity in the β_1AR than the β_2AR. Of note, $F^{45.52}A$ mutation also has larger effects on epinephrine affinity in the β_1AR than the β_2AR, suggesting some common mechanisms of epinephrine and norepinephrine binding to the receptor (Supplementary information, Fig. S12).

Electrostatics distinguish epinephrine and norepinephrine binding
Simulating epinephrine binding to human β_1AR and β_2AR yielded surprisingly similar binding pathways to those of norepinephrine, thus to say, different between the β_1AR and β_2AR (Supplementary information, Fig. S14a–d). The question is why norepinephrine has β_1AR selectivity whereas epinephrine does not. The chemical structures of norepinephrine and epinephrine are very similar except that epinephrine contains an additional methyl group on the primary amine (Fig. 5a). Both ligands are significantly basic (pKa 8.5–8.7[32]) and hence largely exist in a protonated form under physiological conditions. The addition of the methyl group with an electron-donating effect at the amine modifies the electron distribution. According to quantum chemical calculations, the protonated nitrogen of epinephrine (+0.559) is less positively charged than the protonated nitrogen of norepinephrine (+0.631) (Fig. 5a). Due to the charge difference, the molecular electrostatic potential (MEP) of epinephrine is 3.9 kcal/mol smaller compared to norepinephrine along the N-H axis at the distance observed between the N-H hydrogen of the ligands and the negatively charged oxygen of $Asp^{3.32}$ in the crystal structures of β_1AR and β_2AR (1.8 Å), indicating a weaker interaction of epinephrine with negatively charged parts of the receptor (Supplementary information, Fig. S15).

The electrostatic surface map suggests the ligand entrance pathway of the β_1AR contains a continuous negatively charged tunnel. In contrast, the ligand entrance pathway of the β_2AR is composed of two negatively charged areas separated by a neutral gap (Fig. 5b, c). As the protonated nitrogen of norepinephrine is more positively charged than for epinephrine, it may prefer the β_1AR entrance over that of the β_2AR, while epinephrine does not have such a preference. Indeed, even though epinephrine and norepinephrine may take the same binding pathway, they have different binding energy profiles. The norepinephrine binding energy profiles are different between the β_1AR and β_2AR (Fig. 5d; Supplementary information, Fig. S14e), while the epinephrine binding energy profiles show similar patterns between the two receptors (Fig. 5e; Supplementary information, Fig. S14e). Interestingly, norepinephrine seems to be transiently trapped in a pocket located before the orthosteric pocket in the β_2AR (at a collective variable (CV) distance of 1.2 nm) (Fig. 5d, red arrow), which may partially explain the slower association rate to the orthosteric pocket. The binding mode is well maintained for 1275 ns in unbiased MD simulations (Fig. 5f). In binding kinetics studies, epinephrine showed an approximately threefold slower association rate than norepinephrine in the β_1AR, which may be due to both the slightly larger size and the charge distribution difference (Supplementary information, Table S1). While in the β_2AR, epinephrine showed a ~14-fold faster association rate than norepinephrine. Hence, epinephrine appears to migrate faster through the less continuously charged pathway of β_2AR. This agrees with the lower charge and MEP value, produced by the shielding effect of the N-methyl group on the positively charged nitrogen. The epinephrine association rate is only approximately twofold faster in the β_2AR than in the β_1AR, suggesting a similar preference for the extracellular vestibule structures of the β_1AR and β_2AR. Epinephrine binding studies with the $\beta_1AR_{in}/\beta_2AR_{out}$ and the $\beta_2AR_{in}/\beta_1AR_{out}$ chimera receptors indicated that the observed difference in epinephrine association may be contributed by the transmembrane core of the receptor (Supplementary information, Fig. S16, Table S1b). The twofold difference in association rate may be a reflection of subtle differences in the equilibrium between active and inactive states and could partly explain why $\beta_1AR_{in}/\beta_2AR_{out}$ has a faster dissociation rate and lower affinity than the other three receptor variants.

DISCUSSION

We sought to address an interesting and physiologically important difference in the binding affinity of norepinephrine for the human β_1AR and β_2AR. Our results suggest that the selectivity is largely dictated by the association rate of the catecholamine, which might be the key to sympathetic nervous system function. The relatively slow association rate of norepinephrine to the β_2AR might also contribute to the inefficient coupling of β_2AR to Gi and differences in β_2AR trafficking in neonatal cardiac myocytes compared to receptor activated by epinephrine.[9] Crystal structures revealed identical orthosteric catecholamine-binding pockets, but different shapes and electrostatics of the extracellular vestibules of the β_1AR and β_2AR. Metadynamics simulations indicated that the two receptor isoforms have different ligand entrance pathways that account for the association rate difference. Interrogation of the entrance pathway through site-directed mutagenesis suggests that residues within the extracellular vestibule may serve as "selectivity filter" for norepinephrine. Even though epinephrine takes the same binding pathway as norepinephrine, the additional methyl group at its nitrogen alters the electron distribution on the catecholamine. Consequently, epinephrine does not show a preference for the extracellular vestibule of the β_1AR or β_2AR, while norepinephrine is transiently trapped in an intermediate binding site in the extracellular vestibule of the β_2AR due to its higher positive charge density.

The results have a broader implication for drug development where receptors with identical orthosteric pockets could have different selectivity filters that define the pharmacology. Here, the

selectivity filter is defined by the extracellular vestibule, a solvent-accessible tunnel, located above the orthosteric binding site, which is found in many class A GPCRs. Identifying subtype-selective drugs is a major goal in the development of safer and more efficacious therapeutics that target GPCRs. Our data suggest that efforts to develop subtype-selective ligands using structure-based drug design should consider the extracellular vestibule not only in the context of allosteric modulators or bitopic ligands, which bridge both the orthosteric site and the vestibule, but also for smaller orthosteric ligands.

MATERIALS AND METHODS

Human β1AR construct design and expression

In the human T4L–β_1AR construct, T4 lysozyme was connected to $S54^{1.28}$ of β_1AR with two alanine residues and the receptor was truncated at position 399 as previously reported for T4L–β_2AR construct.[33] The flexible ICL3 of T4L–β_1AR (C261–L314) was removed and FLAG epitope (DYKDDDA) was fused to the amino-terminus of T4L–β_1AR. The receptor was expressed in *Sf9* insect cells with recombinant baculovirus (Bac-to-Bac expression systems) for 48 h at 27 °C.

Protein purification

For inactive-state β_1AR structure determination, T4L–β_1AR was solubilized in solubilization buffer (20 mM HEPES, pH 7.5, 100 mM NaCl, 1% LMNG and 0.02% CHS) and purified by M1 Flag affinity chromatography (Sigma) followed with a size exclusion chromatography in a final buffer comprised of 20 mM HEPES, pH 7.5, 100 mM NaCl, 0.01% LMNG, 0.0002% CHS and 10 μM carazolol.

For active-state β_1AR structure determination, Nb6B9 with carboxyl-terminus His tag was expressed in *E. coli* strain BL21 (DE3) and purified by nickel affinity chromatography as previously reported.[28] The T4L–β_1AR was purified by M1 Flag affinity chromatography in presence of the target agonists (100 nM BI-167107, 1 mM epinephrine or 1 mM norepinephrine) and mixed with a 1.2-fold molar excess of Nb6B9 overnight at 4 °C. A nickel affinity chromatography was performed to pull down functional receptor. A final size exclusion chromatography purification was performed to remove excess Nb6B9. The size exclusion chromatography buffer was comprised of 20 mM HEPES, pH 7.5, 100 mM NaCl, 0.01% LMNG and 0.0002% CHS plus target agonists (100 nM BI-167107, 1 mM epinephrine or 1 mM norepinephrine, respectively).

Crystallization of β1AR

Purified protein was reconstituted into lipidic cubic phase by mixing with monoolein (Sigma) containing 10% (w/w) cholesterol (Sigma) in a 2:3 protein to lipid ratio (w/w) using previously reported two-syringe method.[34] The β_1AR–carazolol crystals were grown in 100 mM sodium citrate, pH 5.0, 150 to 175 mM lithium sulfate, 38% to 42% PEG300 and 3% to 6% 1,3-butanediol (Sigma). The β_1AR–BI-167107 crystals were grown in 100 mM HEPES, pH 7.5, 100 to 175 mM ammonium sulfate, 38% to 43% PEG400 and 0.15 to 0.2 M Glycine. β_1AR–norepinephrine and β_1AR–epinephrine crystals were grown in 100 mM HEPES, pH 7.5, 100 to 175 mM sodium sulfate, 38% to 43% PEG300, and 1 mM ligands. Crystals appeared after 1 d and reached full size within 4 d at 20 °C.

Diffraction data collection and processing

The diffraction data was collected with the automatic data collection system ZOO[35] at beamline BL32XU, SPring-8, Japan. The micro-focused beam with 1 Å wavelength and 10 × 15 μm size was used for automatic data collection. For each crystal, 5° or 10° dataset was collected with 0.1° oscillation per frame.

The diffraction data was automatically processed by KAMO.[36] For β_1AR–carazolol dataset, 1038 crystals were merged together to generate the final 2.5 Å dataset. For β_1AR–BI-167107, β_1AR–norepinephrine and β_1AR–epinephrine datasets, 101 crystals, 318 crystals and 94 crystals were used to generate the final datasets, respectively.

Structure determination and refinement

The β1AR–carazolol and β_1AR–BI-167107 structures were solved by molecular replacement using phenix[37] with β_2AR–carazolol (PDB code: 2RH1) and β_2AR–BI-167107 (PDB code: 4LDE) structures as searching models, respectively, while the β_1AR–norepinephrine and β_1AR–epinephrine structures were solved using β_1AR–BI-167107 structure as searching model. Structure refinement was carried out with phenix.refine in combination with manual building in coot.[38] The final structure validations were performed with Molprobity.[39] Statistics for data collection and structure refinement are summarized in Supplementary information, Table S2. All structure figures were prepared using PyMOL (the PyMOL Molecular Graphics System, Schrödinger, LLC).

Radioligand binding on βARs and mutants

The wild-type human β_1AR, β_2AR, $\beta_1AR_{in}/\beta_2AR_{out}$ and $\beta_2AR_{in}/\beta_1AR_{out}$ chimeras and turkey β_1AR constructs were synthesized (GENEWIZ) and subcloned into pFastbac vector. Mutations for the human β_1AR and human β_2AR were generated by site-directed mutagenesis. Receptors were expressed in *Sf9* insect cells with Bac-to-Bac expression system. For membrane preparation, 50 mL cells were centrifuged and homogenized in 8 mL lysis buffer (20 mM Tris, pH 7.5, 1 mM EDTA). The lysate solution was centrifuged at 800 rpm for 10 min. The supernatant was then isolated and centrifuged at 18,000 rpm for 20 min. Finally, the membrane-containing pellet was resuspended with binding buffer (20 mM HEPES, pH 7.5, 100 mM NaCl).

For competition binding assay, 100 μL diluted membrane-suspension was incubated with varying concentrations of cold ligands and 0.15–2 nM [^{3}H]DHA in a buffer containing 20 mM HEPES, pH 7.5, 100 mM NaCl and 0.5 mg/mL BSA, to a final volume of 500 μL and incubated for 1.5 h with shaking at 200 rpm. The membranes were collected by filtration using Brandel 48-well harvester and filter papers containing the membrane were incubated with 3 mL OptiPhase HiSafe 3 liquid scintillation cocktail. The radioactivity was counted by Microbeta2 scintillation counter. Binding curves were fitted by GraphPad Prism 6.0 (GraphPad LLC, CA).

The binding kinetics assay

Dissociation binding kinetics of [^{3}H]-DHA was measured by incubating membranes from *Sf9* insect cells expressing wild-type human β_1AR, β_2AR, $\beta_1AR_{in}/\beta_2AR_{out}$ or $\beta_2AR_{in}/\beta_1AR_{out}$ chimeras with 0.1–0.5 nM [^{3}H]-DHA in assay buffer (20 mM HEPES, pH 7.4, 100 mM NaCl, and 1 mM ascorbic acid) for 1 h, followed by the addition of an equal volume of propranolol (final concentration of 50 μM to prevent re-association of [^{3}H]-DHA) and then harvesting on GF/C Unifilter™ (Perkin-Elmer) plates by vacuum filtration at different time points. The amount of [^{3}H]-DHA bound to the filters was measured by liquid scintillation counting in a Top Count™ (Perkin Elmer) and the dissociation constants were determined using one phase exponential decay fit with GraphPad Prism 6.0 (GraphPad LLC, CA). Association binding kinetics were measured by incubating membranes with 3 different concentrations of [^{3}H]-DHA (0.1–0.5 nM) for different times and determining the association binding constants using GraphPad Prism 6.0 (GraphPad LLC, CA). To determine the binding kinetics of unlabeled agonists, competition association assays were performed as previously described.[40] Membranes were incubated with at least 3 different concentrations of the unlabeled agonist and a single concentration of [^{3}H]-DHA (0.1–0.5 nM) for different times. Binding kinetics of the agonists were determined using the Kinetics of

Competitive Binding fit in GraphPad Prism 6.0 (GraphPad LLC, CA) using the measured kinetic parameters for [^{3}H]-DHA in the analysis.

β-arrestin-2 recruitment assay

The β-arrestin-2 recruitment assay was performed using the PathHunter assay (DiscoverX, Birmingham, UK). In general, HEK293 cells stably expressing (EA)-β-arrestin-2 were transiently transfected with a receptor containing the PK fragment tag using Mirus TransIT-293 (peqlab, Erlangen, Germany). After 24 h incubation in DMEM/F12 medium (Life Technologies, Darmstadt, Germany) at 37 °C and 5% of CO_2, the cells were detached and transferred into 384-well plates at around 5000 cells/well density. After incubation for another 24 h, the catecholamines were added to the cell and incubated at 37 °C for an optimized time for each receptor. The detection mix was added and incubated at room temperature for 1 h. The chemoluminescence measurement for β-arrestin-2 recruitment was performed with a Clariostar plate reader (BMG, Ortenberg, Germany).

Setup of MD simulations

The simulations of the active state are based on the here reported crystal structures of β_1AR in complex with norepinephrine and epinephrine or based on the β_2AR crystal structure in complex with epinephrine (PDB code: 4LDO).[28] For β_2AR in complex with norepinephrine, the β_2AR crystal structure in complex with epinephrine was applied. The structure was aligned with the active state structure of β_1AR in complex with norepinephrine and the coordinates of norepinephrine were transferred. For the simulations systems of the inactive state used for the metadynamics simulations, the crystal structures of β_1AR in complex with carazolol (reported here) and β_2AR in complex with carazolol (PDB code: 2RH1)[18] were applied. If simulated in complex with norepinephrine, the respective structure was aligned with the active state structure of β_1AR in complex with norepinephrine and the coordinates of norepinephrine were transferred. In the case of simulations with epinephrine, either the coordinates of epinephrine in the crystal structure of β_1AR or β_2AR were used.

The structures were modified that they cover the same part of the protein sequence. The structures used for β_1AR simulations covered the residues from number 54 to 256 and 318 to 391 and the structures used for β_2AR simulations covered the residues from number 29 to 231 and 367 to 340. Missing side chains were completed utilizing UCSF Chimera[41] and a palmitoyl group was added to Cys392 or Cys341 according to the UniProt entry of human β_1AR[42] and β_2AR,[43] respectively. The open N- and C-termini, as well as the terminal residues at the intracellular ends of TM5 and 6, were capped with neutral acetyl and methylamide groups.

For simulations of active states, all titratable residues were left in their dominant protonation state at pH 7.0 except for Asp$^{2.50}$, Glu$^{3.41}$ and Asp$^{3.49}$. Previous studies of the β_2AR suggest that Asp$^{2.50}$ and Asp$^{3.49}$ are protonated in the active state,[44,45] and residue Glu$^{3.41}$ directly contacts the lipid interface and therefore will also exist predominantly in its protonated state.[46,47] We thus protonated these three residues in our simulations of the active state. For the simulation of inactive states, all titratable residues were left in their dominant protonation state at pH 7.0 except for Glu$^{3.41}$, which was protonated in these simulations as well.

The protein structures were then aligned to the Orientation of Proteins in Membranes (OPM)[48] structure of either active β_2AR (PDB code: 3SN6) for simulations of the active state, or aligned to the structure of inactive β_2AR (PDB code: 2RH1) for simulations of the inactive state. Each complex was inserted into a solvated and pre-equilibrated membrane of dioleoyl-phosphatidylcholine (DOPC) lipids using the GROMACS tool g_membed.[49] Subsequently, water molecules were replaced by sodium and chloride ions to give a neutral system with 0.15 M NaCl. For active state simulations, the final system dimensions were roughly $80 \times 80 \times 120$ Å^3, containing about 150 lipids, about 17.500 water molecules, 71 sodium ions and 88 or 78 chloride ions for β_1AR and β_2AR, respectively. In the case of simulations of the inactive state, the final system dimensions were roughly $80 \times 80 \times 100$ Å^3, containing about 150 lipids, about 13.000 water molecules, 59 sodium ions and 73 or 64 chloride ions for β_1AR and β_2AR, respectively.

Parameter topology and coordinate files were built up using the tleap module of AMBER18[50] and subsequently converted into GROMACS input files. For all simulations, the general AMBER force field (GAFF)[51] was used for the ligands, the lipid14 force field[52] for the DOPC molecules and ff14SB[53] for the protein residues. The SPC/E water model[54] was applied. Parameters for norepinephrine and epinephrine were assigned using antechamber.[50] The structure of norepinephrine and epinephrine were optimized using Gaussian 16[55] at the B3LYP/6-31G(d) level of theory and charges calculated at HF/6-31G(d) level of theory. Subsequently, atom point charges were assigned according to the RESP procedure described in literature.[54] A formal charge of +1 was defined for norepinephrine and epinephrine.

MD simulations

Unbiased simulations were performed using GROMACS 2019.3.[56,57] Multiple simulations were started. Each simulation system was energy minimized and equilibrated in the NVT ensemble at 310 K for 1 ns followed by the NPT ensemble for 1 ns with harmonic restraints of 10.0 kcal·mol^{-1} on protein and ligands. In the NVT ensemble, the V-rescale thermostat was used. In the NPT ensemble the Berendsen barostat, a surface tension of 22 dyn·cm^{-1}, and a compressibility of 4.5×10^{-5} bar^{-1} was applied. The system was further equilibrated for 25 ns with restraints on protein backbone and ligand atoms. Here, the restraints were reduced in a stepwise fashion to be 10.0, 5.0, 1.0, 0.5 and 0.1 kcal·mol^{-1}, respectively. Productive simulations were performed using periodic boundary conditions and a time step of 2 fs with bonds involving hydrogen constrained using LINCS.[58] Long-range electrostatic interactions were computed using the particle mesh Ewald (PME)[59] method with interpolation of order 4 and fast Fourier transform (FFT) grid spacing of 1.6 Å. Non-bonded interactions were cut off at 12.0 Å.

Analysis of the trajectories was performed using Visual Molecular Dynamics (VMD),[60] and the CPPTRAJ[61] module of AMBER18. Visualization was performed using PyMOL (the PyMOL Molecular Graphics System, Schrödinger, LLC). Plots were created using Matplotlib 3.0.2.[62]

Metadynamics simulations

Metadynamics simulations were performed to obtain the free energy profile of norepinephrine and epinephrine at the β_1AR and β_2AR aiming to derive meta-stable intermediate states suggesting a potential binding pathway of the two ligands. The simulations were performed using an inactive state structure of the respective receptor. The simulations were performed using GROMACS 2018.4[56,57] patched with the open-source, community-developed PLUMED library,[63] version 2.5[64] and follows a recently described protocol by Saleh and coworkers to determine ligand binding modes at GPCRs.[29] In brief, we used a combination of the well-tempered metadynamics (WT)[65,66] and funnel-shaped walls. Following the above-described equilibration protocol, a metadynamics-history-dependent bias was applied along with the z component of the distance between the center of mass of the Cα atoms of Val$^{3.36}$ and Trp$^{6.48}$, representing the center of the receptor, and center of mass of the ligand atoms. This distance was used as a single collective variable. A funnel restraint was applied to the relative position on the xy plane to ensure better sampling for the relevant region. Gaussian hills with an initial height of 0.48 kcal·mol^{-1} applied every 1 ps were used. The hill

width was chosen to be 1 Å. The Gaussian functions were rescaled in the WT scheme using a bias factor of 20. For each simulation system, an initial metadynamics simulation was performed until the ligand was unbound from the receptor. Using 16 frames extracted from this initial simulation, a multiple-walker metadynamics simulation was performed. For all systems, these frames cover a spectrum of ligand conformations ranging from the ligand in the orthosteric pocket to the ligand at the extracellular side of the receptor. The free energies were calculated using the sum_hills function of the PLUMED plugin[64] and plotted against the distance of the CV using Matplotlib 3.0.2.[62] For each distance representing a minimum or maximum on the free energy landscape, coordinates were extracted and clustered into ten groups based on the ligand atoms only using the CPPTRAJ[61] module of AMBER18. Representative structures of a cluster were considered as potential meta-stable intermediate states if the cluster included at least 10% of the analyzed frames.

Charge and MEP calculations

The structure of norepinephrine and epinephrine were optimized, and charges were calculated using Gaussian 16[55] at the MP2/aug-cc-pVDZ[67–69] level of theory. The partial charges of the protonated nitrogens present the electrostatic potential charges with charges of hydrogens summed into heavy atoms. The molecular electrostatic potentials were visualized using UCSF Chimera.[41]

DATA AVAILABILITY

The coordinates and structures factors of T4L–β_1AR/carazolol, T4L–β_1AR/Nb6B9/BI-167107, T4L–β_1AR/Nb6B9/norepinephrine and T4L–β_1AR/Nb6B9/epinephrine structures have been deposited in Protein Data Bank under accession number 7BVQ, 7BU7, 7BU6 and 7BTS, respectively.

ACKNOWLEDGEMENTS

We gratefully acknowledge the compute resources and support provided by the Erlangen Regional Computing Center (RRZE) and support provided by Radioisotope Laboratory, Center of Biomedical Analysis, Tsinghua University. This work was supported by the Beijing Advanced Innovation Center for Structural Biology, Tsinghua University (X.X. and X.L.), by the DFG grant GRK 1910 (P.G. and J.K.), National Institute of General Medical Sciences GM106990 (B.K.K., P.G. and R.K.S.) and GM083118 (B.K.K. and R.K.S). B.K.K. is a Chan Zuckerberg Biohub investigator and an Einstein BIH Visiting Fellow.

AUTHOR CONTRIBUTIONS

X.X. performed β_1AR expression, purification and crystallization. X.X. and X.L. performed structure determination and refinement. J.K. performed MD simulations, charge and MEP calculations supervised by P.G. X.X., X.L., H.H. and M.J.C. characterized the pharmacology properties of βARs and mutants. M.J.C. performed the binding kinetics assays supervised by R.K.S. K.H. performed automatic data collection and processing. The paper was written by B.K.K. and X.L., with input from X. X. and J.K., and editing and suggestions from P.G. and R.K.S. B.K.K. coordinated the experiments and supervised the overall research. All authors contributed to the editing of the paper.

ADDITIONAL INFORMATION

Supplementary information accompanies this paper at https://doi.org/10.1038/s41422-020-00424-2.

Competing interests: B.K.K. is a co-founder of and consultant for ConfometRx, Inc. The other authors declare no competing financial interests.

REFERENCES

1. Ablad, B. et al. Cardiac effects of beta-adrenergic receptor antagonists. *Adv. Cardiol.* **12**, 290–302 (1974).
2. Shcherbakova, O. G. et al. Organization of beta-adrenoceptor signaling compartments by sympathetic innervation of cardiac myocytes. *J. Cell Biol.* **176**, 521–533 (2007).
3. Rybin, V. O., Xu, X., Lisanti, M. P. & Steinberg, S. F. Differential targeting of beta -adrenergic receptor subtypes and adenylyl cyclase to cardiomyocyte caveolae. A mechanism to functionally regulate the cAMP signaling pathway. *J. Biol. Chem.* **275**, 41447–41457 (2000).
4. Xiang, Y., Devic, E. & Kobilka, B. The PDZ binding motif of the beta 1 adrenergic receptor modulates receptor trafficking and signaling in cardiac myocytes. *J. Biol. Chem.* **277**, 33783–33790 (2002).
5. Xiang, Y. & Kobilka, B. The PDZ-binding motif of the beta2-adrenoceptor is essential for physiologic signaling and trafficking in cardiac myocytes. *Proc. Natl. Acad. Sci. USA* **100**, 10776–10781 (2003).
6. Perez-Schindler, J., Philp, A. & Hernandez-Cascales, J. Pathophysiological relevance of the cardiac beta2-adrenergic receptor and its potential as a therapeutic target to improve cardiac function. *Eur. J. Pharmacol.* **698**, 39–47 (2013).
7. de Lucia, C., Eguchi, A. & Koch, W. J. New insights in cardiac beta-adrenergic signaling during heart failure and aging. *Front. Pharmacol.* **9**, 904 (2018).
8. Devic, E., Xiang, Y., Gould, D. & Kobilka, B. Beta-adrenergic receptor subtype-specific signaling in cardiac myocytes from beta(1) and beta(2) adrenoceptor knockout mice. *Mol. Pharmacol.* **60**, 577–583 (2001).
9. Wang, Y. et al. Norepinephrine- and epinephrine-induced distinct beta2-adrenoceptor signaling is dictated by GRK2 phosphorylation in cardiomyocytes. *J. Biol. Chem.* **283**, 1799–1807 (2008).
10. Wortsman, J., Frank, S. & Cryer, P. E. Adrenomedullary response to maximal stress in humans. *Am. J. Med.* **77**, 779–784 (1984).
11. Zhu, W. Z. et al. Linkage of beta1-adrenergic stimulation to apoptotic heart cell death through protein kinase A-independent activation of Ca2+/calmodulin kinase II. *J. Clin. Invest.* **111**, 617–625 (2003).
12. Lymperopoulos, A., Rengo, G. & Koch, W. J. Adrenergic nervous system in heart failure: pathophysiology and therapy. *Circ. Res.* **113**, 739–753 (2013).
13. Chesley, A. et al. The beta(2)-adrenergic receptor delivers an antiapoptotic signal to cardiac myocytes through G(i)-dependent coupling to phosphatidylinositol 3′-kinase. *Circ. Res.* **87**, 1172–1179 (2000).
14. Zhu, W. Z. et al. Dual modulation of cell survival and cell death by beta(2)-adrenergic signaling in adult mouse cardiac myocytes. *Proc. Natl. Acad. Sci. USA* **98**, 1607–1612 (2001).
15. Bernstein, D. et al. Differential cardioprotective/cardiotoxic effects mediated by beta-adrenergic receptor subtypes. *Am. J. Physiol. Heart Circ. Physiol.* **289**, H2441–H2449 (2005).
16. Goldspink, D. F., Burniston, J. G. & Tan, L. B. Cardiomyocyte death and the ageing and failing heart. *Exp. Physiol.* **88**, 447–458 (2003).
17. Rasmussen, S. G. et al. Crystal structure of the human beta2 adrenergic G-protein-coupled receptor. *Nature* **450**, 383–387 (2007).
18. Cherezov, V. et al. High-resolution crystal structure of an engineered human beta2-adrenergic G protein-coupled receptor. *Science* **318**, 1258–1265 (2007).
19. Rosenbaum, D. M. et al. GPCR engineering yields high-resolution structural insights into beta2-adrenergic receptor function. *Science* **318**, 1266–1273 (2007).
20. Warne, T. et al. Structure of a beta1-adrenergic G-protein-coupled receptor. *Nature* **454**, 486–491 (2008).
21. Warne, T., Edwards, P. C., Dore, A. S., Leslie, A. G. W. & Tate, C. G. Molecular basis for high-affinity agonist binding in GPCRs. *Science* **364**, 775–778 (2019).
22. Baker, J. G. A full pharmacological analysis of the three turkey beta-adrenoceptors and comparison with the human beta-adrenoceptors. *PLoS One* **5**, e15487 (2010).
23. Masureel, M. et al. Structural insights into binding specificity, efficacy and bias of a beta2AR partial agonist. *Nat. Chem. Biol.* **14**, 1059–1066 (2018).
24. Strasser, A., Wittmann, H. J. & Seifert, R. Binding kinetics and pathways of ligands to GPCRs. *Trends Pharmacol. Sci.* **38**, 717–732 (2017).
25. Engelhardt, S., Grimmer, Y., Fan, G. H. & Lohse, M. J. Constitutive activity of the human beta(1)-adrenergic receptor in beta(1)-receptor transgenic mice. *Mol. Pharmacol.* **60**, 712–717 (2001).
26. Rasmussen, S. G. et al. Structure of a nanobody-stabilized active state of the beta (2) adrenoceptor. *Nature* **469**, 175–180 (2011).
27. Rasmussen, S. G. et al. Crystal structure of the beta2 adrenergic receptor-Gs protein complex. *Nature* **477**, 549–555 (2011).
28. Ring, A. M. et al. Adrenaline-activated structure of beta2-adrenoceptor stabilized by an engineered nanobody. *Nature* **502**, 575–579 (2013).
29. Saleh, N., Ibrahim, P., Saladino, G., Gervasio, F. L. & Clark, T. An efficient metadynamics-based protocol to model the binding affinity and the transition state ensemble of G-protein-coupled receptor ligands. *J. Chem. Inf. Model.* **57**, 1210–1217 (2017).
30. DeVree, B. T. et al. Allosteric coupling from G protein to the agonist-binding pocket in GPCRs. *Nature* **535**, 182–186 (2016).
31. Dror, R. O. et al. Pathway and mechanism of drug binding to G-protein-coupled receptors. *Proc. Natl. Acad. Sci. USA* **108**, 13118–13123 (2011).
32. Alvarez-Diduk, R. & Galano, A. Adrenaline and noradrenaline: protectors against oxidative stress or molecular targets? *J. Phys. Chem. B* **119**, 3479–3491 (2015).

33. Zou, Y., Weis, W. I. & Kobilka, B. K. N-terminal T4 lysozyme fusion facilitates crystallization of a G protein coupled receptor. *PLoS One* **7**, e46039 (2012).
34. Caffrey, M. & Cherezov, V. Crystallizing membrane proteins using lipidic mesophases. *Nat. Protoc.* **4**, 706–731 (2009).
35. Hirata, K. et al. ZOO: an automatic data-collection system for high-throughput structure analysis in protein microcrystallography. *Acta Crystallogr. D Struct. Biol.* **75**, 138–150 (2019).
36. Yamashita, K., Hirata, K. & Yamamoto, M. KAMO: towards automated data processing for microcrystals. *Acta Crystallogr. D Struct. Biol.* **74**, 441–449 (2018).
37. Adams, P. D. et al. PHENIX: a comprehensive Python-based system for macromolecular structure solution. *Acta Crystallogr. D Biol. Crystallogr.* **66**, 213–221 (2010).
38. Emsley, P., Lohkamp, B., Scott, W. G. & Cowtan, K. Features and development of Coot. *Acta Crystallogr. D Biol. Crystallogr.* **66**, 486–501 (2010).
39. Chen, V. B. et al. MolProbity: all-atom structure validation for macromolecular crystallography. *Acta Crystallogr. D Biol. Crystallogr.* **66**, 12–21 (2010).
40. Guo, D. et al. Dual-point competition association assay: a fast and high-throughput kinetic screening method for assessing ligand-receptor binding kinetics. *J. Biomol. Screen.* **18**, 309–320 (2013).
41. Pettersen, E. F. et al. UCSF Chimera-a visualization system for exploratory research and analysis. *J. Comput. Chem.* **25**, 1605–1612 (2004).
42. UniProt Consortium. UniProtKB—P08588 (ADRB1_HUMAN); https://www.uniprot.org/uniprot/P08588 (2019).
43. UniProt Consortium. UniProtKB—P07550 (ADRB2_HUMAN); https://www.uniprot.org/uniprot/P07550 (2019).
44. Ghanouni, P. et al. The effect of pH on beta(2) adrenoceptor function. Evidence for protonation-dependent activation. *J. Biol. Chem.* **275**, 3121–3127 (2000).
45. Ranganathan, A., Dror, R. O. & Carlsson, J. Insights into the role of Asp79(2.50) in beta2 adrenergic receptor activation from molecular dynamics simulations. *Biochemistry* **53**, 7283–7296 (2014).
46. Dror, R. O. et al. Identification of two distinct inactive conformations of the beta2-adrenergic receptor reconciles structural and biochemical observations. *Proc. Natl. Acad. Sci. USA* **106**, 4689–4694 (2009).
47. Rosenbaum, D. M. et al. Structure and function of an irreversible agonist-beta(2) adrenoceptor complex. *Nature* **469**, 236–240 (2011).
48. Lomize, M. A., Lomize, A. L., Pogozheva, I. D. & Mosberg, H. I. OPM: orientations of proteins in membranes database. *Bioinformatics* **22**, 623–625 (2006).
49. Wolf, M. G., Hoefling, M., Aponte-Santamaria, C., Grubmuller, H. & Groenhof, G. g_membed: efficient insertion of a membrane protein into an equilibrated lipid bilayer with minimal perturbation. *J. Comput. Chem.* **31**, 2169–2174 (2010).
50. Case, D. A. et al. *AMBER18*. (University of California, San Francisco, 2018).
51. Wang, J., Wolf, R. M., Caldwell, J. W., Kollman, P. A. & Case, D. A. Development and testing of a general amber force field. *J. Comput. Chem.* **25**, 1157–1174 (2004).
52. Dickson, C. J. et al. Lipid14: the amber lipid force field. *J. Chem. Theory Comput.* **10**, 865–879 (2014).
53. Maier, J. A. et al. ff14SB: improving the accuracy of protein side chain and backbone parameters from ff99SB. *J. Chem. Theory Comput.* **11**, 3696–3713 (2015).
54. Bayly, C. I., Cieplak, P., Cornell, W. & Kollman, P. A. A well-behaved electrostatic potential based method using charge restraints for deriving atomic charges: the RESP model. *J. Phys. Chem.* **97**, 10269–10280 (1993).
55. Frisch, M. J. et al. *Gaussian 16 Rev. B.01*. (Wallingford, CT, 2016).
56. Van Der Spoel, D. et al. GROMACS: fast, flexible, and free. *J. Comput. Chem.* **26**, 1701–1718 (2005).
57. Abraham, M. J. et al. GROMACS: high performance molecular simulations through multi-level parallelism from laptops to supercomputers. *SoftwareX* **1–2**, 19–25 (2015).
58. Hess, B., Bekker, H., Berendsen, H. J. C. & Fraaije, J. G. E. M. LINCS: a linear constraint solver for molecular simulations. *J. Comput. Chem.* **18**, 1463–1472 (1997).
59. Darden, T., York, D. & Pedersen, L. Particle Mesh Ewald—an N.Log(N) method for Ewald sums in large systems. *J. Chem. Phys.* **98**, 10089–10092 (1993).
60. Humphrey, W., Dalke, A. & Schulten, K. VMD: visual molecular dynamics. *J. Mol. Graph* **14**, 33–38 (1996).
61. Roe, D. R. & Cheatham, T. E. 3rd PTRAJ and CPPTRAJ: software for processing and analysis of molecular dynamics trajectory data. *J. Chem. Theory Comput.* **9**, 3084–3095 (2013).
62. Hunter, J. D. Matplotlib: a 2D graphics environment. *Comp. Sci. Eng.* **9**, 90–95 (2007).
63. Bonomi, M. et al. Promoting transparency and reproducibility in enhanced molecular simulations. *Nat. Methods* **16**, 670–673 (2019).
64. Tribello, G. A., Bonomi, M., Branduardi, D., Camilloni, C. & Bussi, G. PLUMED 2: new feathers for an old bird. *Comput. Phys. Commun.* **185**, 604–613 (2014).
65. Laio, A. & Parrinello, M. Escaping free-energy minima. *Proc. Natl. Acad. Sci. USA* **99**, 12562–12566 (2002).
66. Barducci, A., Bussi, G. & Parrinello, M. Well-tempered metadynamics: a smoothly converging and tunable free-energy method. *Phys. Rev. Lett.* **100**, 020603 (2008).
67. Pople, J. A., Binkley, J. S. & Seeger, R. Theoretical models incorporating electron correlation. *Int. J. Quant. Chem.* **10**, 1–19 (1976).
68. Dunning, T. H. Gaussian basis sets for use in correlated molecular calculations. I. The atoms boron through neon and hydrogen. *J. Chem. Phys.* **90**, 1007–1023 (1989).
69. Kendall, R. A., Dunning, T. H. & Harrison, R. J. Electron affinities of the first-row atoms revisited. Systematic basis sets and wave functions. *J. Chem. Phys.* **96**, 6796–6806 (1992).